C. R. Acad. Sci. Paris, t. 1, Série IV, p. 1065–1081, 2000
Électromagnétisme, optique/*Electromagnetism, optics*
(Gaz, plasmas/*Gas, plasmas*)

LES DÉVELOPPEMENTS RÉCENTS DES LASERS À RAYONS X

RECENT PROGRESS IN X-RAY LASERS

Capillary discharge tabletop soft X-ray lasers reach new wavelengths and applications

J.-J. ROCCA [a], M. FRATI [a], B. BENWARE [a], M. SEMINARIO [a], J. FILEVICH [a,1], M. MARCONI [a,1], K. KANIZAY [a], A. OZOLS [a], I.A. ARTIUKOV [b], A. VINOGRADOV [b], Y.A. USPENSKII [b]

[a] Department of Electrical and Computer Engineering. Colorado State University, Fort Collins, CO 80523, USA
[b] Lebedev Physical Institute, Moscow, 117924 Russia

(Reçu le 29 mai 2000, accepté le 15 juin 2000)

Abstract. For many years, researchers have envisioned the development of compact high repetition rate tabletop soft X-ray lasers that could be routinely used in application in numerous disciplines. With demonstrated average powers of several mW and mJ-level pulse energy at 46.9 nm, capillary discharge-pumped lasers are the first compact lasers to reach this goal. In this paper we summarize the development status of high repetition rate tabletop soft X-ray lasers based on capillary discharge excitation, and give examples of their successful use in several applications. Results of the use of a capillary discharge pumped 46.9 nm laser in dense plasma interferometry, soft X-ray reflectometry for the determination of optical constants, and laser ablation are described. The observation of lasing at 53 nm line in Ne-like Cl with output pulse energy up to 10 μJ is also reported. © 2000 Académie des sciences/Éditions scientifiques et médicales Elsevier SAS

tabletop soft X-ray lasers

Vers de nouvelles longueurs d'onde et applications pour les lasers X–UV compacts à décharge capillaire

Résumé. *Depuis de nombreuse années, les chercheurs prévoient le développement de laser X–UV compacts, dits « de table », qui pourraient être utilisés en routine pour les applications à des disciplines variées. Avec des puissances moyennes mesurées de plusieurs* mW *et une énergie par impulsion au niveau du millijoule à* 46.9 nm, *les lasers pompés par décharge capillaire sont les premiers lasers compacts à atteindre ce but. Dans cet article, nous résumons l'état de l'art des lasers X–UV à haut taux de répétition basés sur l'excitation par décharge capillaire et nous donnons des exemples de leur utilisation réussie dans plusieurs applications. Nous décrirons successivement l'utilisation d'un laser à* 46.9 nm *pompé par décharge pour l'interférométrie d'un plasma dense, la mesure des constantes optiques par réflectométrie X–UV et l'ablation par laser X–UV. On montrera également l'observation d'un effet laser à* 53 nm *dans le chlore néonoïde avec une énergie par impulsion de* 10 μJ. *© 2000 Académie des sciences/Éditions scientifiques et médicales Elsevier SAS*

lasers X–UV compacts

Note présentée par Guy LAVAL.

S1296-2147(00)01113-6/FLA
© 2000 Académie des sciences/Éditions scientifiques et médicales Elsevier SAS. Tous droits réservés.

1. Introduction

There are strong motivations for the development of compact sources of coherent soft X-ray radiation that will allow soft X-ray science in a tabletop environment. Schemes based on the non-linear optical techniques for frequency up-conversion of optical laser radiation [1,2], and different approaches for the direct amplification of spontaneous emission in a plasma (soft X-ray lasers) [3] are currently under development. Capillary discharge excitation of elongated Ne-like Ar plasma columns is the first technology to reach mW average powers of coherent soft X-ray radiation and millijoule-level pulses in a tabletop set up. Multi-hertz repetition rate operation generated an average power of ≈ 3.5 mW at a wavelength of 46.9 nm [4]. The advanced degree of development of this laser is summarized in Section 2.

There is also significant interest in extending the availability of practical discharge-pumped short wavelength lasers to other wavelengths. In particular, applications in photochemistry and photophysics can significantly benefit from repetitive laser sources of high energy photons that are capable of causing single-photon ionization of all neutral species, yet fall short of the 24.6 eV threshold for the photoionization of He. In Section 3 we discuss the generation of laser pulses at 52.9 nm (23.4 eV) in the $3p$–$3s$ $J = 0$–1 line of Ne-like Cl utilizing a compact capillary discharge. Section 4 of the paper is devoted to review recent results of the use of capillary discharge lasers in applications, and is organized as follows: Section 4.1 discusses the demonstration of plasma interferometry with a 46.9 nm tabletop laser and a novel Mach–Zehnder interferometer based on diffraction gratings, Section 4.2 summarizes results of soft X-ray reflectometry measurements that resulted in the determination of optical constants of several materials and Section 4.3 reviews the first demonstration of laser ablation with a soft X-ray laser.

2. Development status of the 46.9 nm Ne-like Ar tabletop laser: demonstration of milliwatt average power and millijoule-level pulses

The Ne-like Ar capillary discharge laser is perhaps the most mature of all the tabletop soft X-ray lasers developed to date. *Table 1* summarizes the characteristics of this laser and its present output parameters. These laser output parameters were obtained utilizing aluminum oxide capillary channels 3.2 mm in diameter filled with preionized Ar gas at an optimized pressure of ≈ 460 mTorr. The plasma columns were excited by current pulses of ≈ 26 kA peak amplitude with a 10% to 90% rise time of approximately 40 ns. *Figure 1* illustrates the size of the capillary discharge Ne-like Ar laser. This capillary discharge-pumped laser occupies a table space of approximately 0.4 m $\times$ 1 m on top of a table, a size comparable to that of many widely utilized visible or ultraviolet gas lasers. In this laser the excitation current pulse is produced by discharging a water capacitor through a spark gap switch connected in series with the capillary load. The water served as a liquid dielectric for the capacitor and also cooled the capillary. The capacitor is pulse-charged by a compact Marx generator.

The laser average output pulse energy was measured to increase from 0.075 mJ for a plasma column 16 cm in length, to 0.88 mJ for the plasma column 34.5 cm in length. Estimates of the laser intensity

Table 1. Summary of 46.9 nm Ne-Like Ar capillary discharge table-top soft X-ray laser parameters

Laser parameter		Ref.
Pulse energy	0.88 mJ @ 4 Hz	[4]
Average pulse power	3.5 mW	[4]
Peak pulse power	0.6 MW	[4,5]
Divergence	≈ 4.6 mrad	[4,5]
Pulse width	1.2–1.5 ns	[6]
Pulse spectral brightness	$2 \cdot 10^{25}$ photons/(s·mm^2·mrad^2·0.01% bandwidth)	[4]

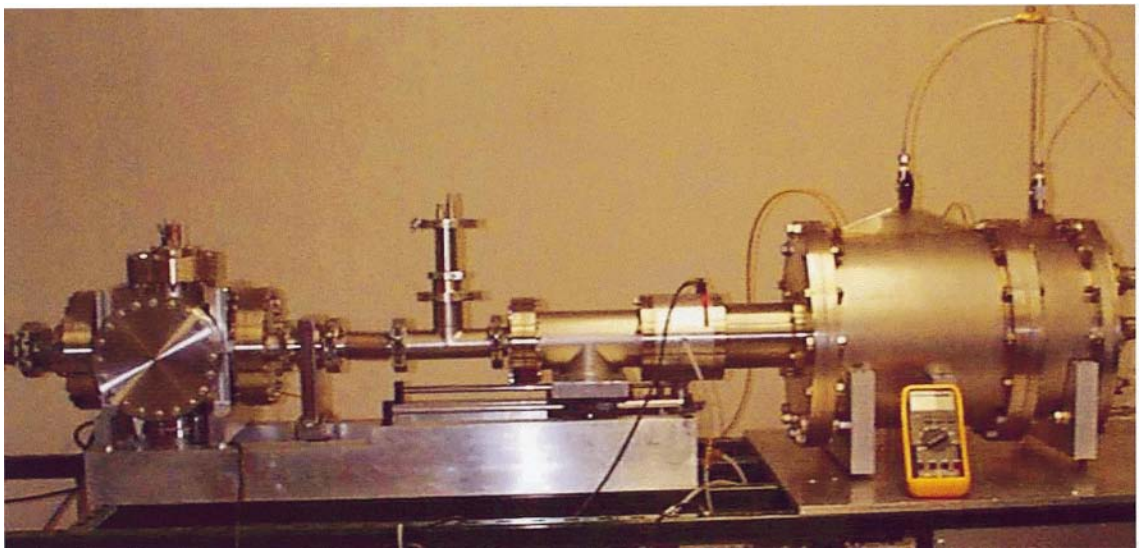

Figure 1. Photograph of capillary discharge soft X-ray laser (right) and applications chamber (left). The Multimeter that is shown in front of the laser to provide size reference.

based on these energies, and on laser pulse-width measurements indicate that the saturation intensity is exceeded before the end of the 16 cm capillary, and that the output of the longest capillary exceeds the saturation intensity by more than an order of magnitude, approaching 1 $\mathrm{GW/cm^2}$. *Figure 2a* shows the shot to shot variations of the measured laser output pulse energy and corresponding laser average power for a 34.5 cm long discharge operated at 4 Hz repetition frequency. The average laser power is about 3.5 mW, corresponding to $> 8 \cdot 10^{14}$ photons per second. *Figure 2b* shows the average laser output energy per pulse is 0.88 mJ and that the energy of the highest energy pulses exceeds 1 mJ. More than 5000 laser shots were obtained from a single capillary. The full width at half maximum of the corresponding laser pulse is 1.5 ± 0.05 ns. This laser pulse-width is longer than the 1.2 ns that we measured for an 18.2 cm long amplifier [5]. Taking into consideration this pulse-width, the average peak laser output power obtained with the longest plasma column is estimated to be ≈ 0.6 MW. The peak to peak divergence was measured to be about 4.6 mrad for all capillary lengths between 18 and 34.5 cm. Recent measurements of the spatial coherence indicate that full spatial coherence is approached with the longest capillaries and that the peak spectral brightness is about $2 \cdot 10^{25}$ photons/(s·$\mathrm{mm^2}$·$\mathrm{mrad^2}$·0.01% bandwidth) [6]. This value makes this table-top laser one of the brightest soft X-ray sources available.

This demonstration of a table-top soft X-ray laser with a spatially coherent average power per unit bandwidth similar to that of a synchrotron beam-line and laser pulse energies approaching 1 mJ has the potential to greatly expand the use of intense coherent short-wavelength radiation in applications. Latter in this paper we summarize the successful application of this laser to the diagnostics of plasmas and to the processing and characterization of material surfaces.

3. Demonstration at 52.9 nm capillary discharge laser in Ne-like Cl

There is also significant interest in extending the availability of practical saturated tabletop short wavelength lasers to different regions of the spectrum. In particular, applications in photochemistry and photophysics can significantly benefit from repetitive laser sources of high energy photon that are capable of causing single-photon ionization of neutral species, yet fall short of the 24.6 eV threshold for the

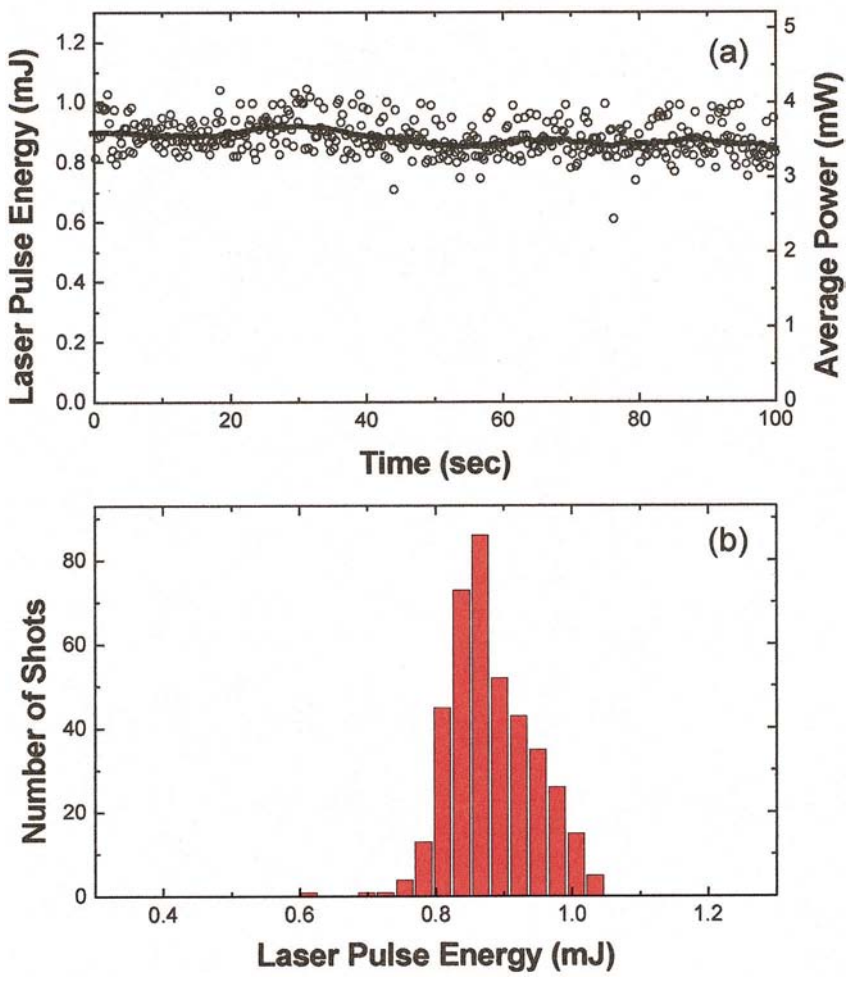

Figure 2. Measured output pulse energy and average power of a table-top capillary discharge 46.9 nm laser operating at a repetition frequency of 4 Hz. (a) Shot-to shot laser output energy and average output power computed as a walking average of 60 continuous laser pulses. (b) Distribution of the output pulse energy. Average pulse energy is 0.88 mJ and the standard deviation is 0.06 mJ.

photoionization of He. These applications include the study of nanoclusters created by optical laser ablation, a technique that uses He as a carrier gas [7].

We have demonstrated the generation of laser pulses at 52.9 nm (23.4 eV) in the $3p^1S_0$–s^1P_1 transition of Ne-like Cl utilizing a very compact tabletop capillary discharge [8]. Laser amplification of this line was previously observed by Y. Li et al. in a plasma generated by exciting a solid KCl target with 450 ± 20 J laser pulses of 0.45 ns duration produced by the powerful Asterix iodine laser facility at a rate of several shots per hour [9]. In that experiment the amplification obtained in a 3 cm long plasma ($g \times l \sim 7.5$) was far below that required to reach gain saturation, limiting the laser pulse output energy to relatively low values. In the 18.2 cm long discharge-pumped plasma column used in the tabletop experiments reported herein the amplified spontaneous emission intensity reached values of the order of the saturation intensity, allowing for the generation of a significantly greater laser output pulse energy. Laser pulses with energy up to 10 μJ were measured operating the discharge at repetition rates between 0.5 and 1 Hz.

The gain media was generated by rapidly exciting a 3.2 mm inside diameter aluminum oxide capillary channel filled with pre-ionized chlorine gas with a fast current pulse. The capillary discharge set up utilized in the experiment is similar to that previously used to obtain lasing in Ne-like Ar at high repetition rates [5]. Amplification was observed at Cl_2 pressures ranging from 180 to 300 mTorr. The plasma columns were excited by current pulses of approximately 23 kA peak amplitude, 10–90% rise-time of approximately 25 ns, and first half cycle duration of 110 ns. In this discharge, the fast current pulse rapidly compresses the plasma creating a small diameter column [10,11] in which monopole collisional electron excitation of Ne-like Cl ions creates a large population inversion between the $3p^1S_0$ and $3s^1P_1$ levels, resulting in strong amplification at 52.9 nm. Cl_2 was continuously admitted into the capillary channel using chemically compatible teflon tubing and stainless steel fittings. The gas was pumped using a rotary vane pump containing perfluoropolyether oil and turbomolecular pumps purged with N_2.

Spectral diagnostic was implemented utilizing a 1 m focal length normal incidence spectrograph containing a 600 l/mm diffraction grating and micro-channel plate (MCP) intensified charged-coupled device (CCD) detector array. *Figure 3* shows spectra of the axial emission of the discharge, covering a 40 nm region in the vicinity of the $J = 0$–1 laser line of Ne-like Cl. The spectrum obtained at a pressure of 120 mTorr (*figure 3a*), shows line emission at the 52.9 nm wavelength of the laser transition. However,

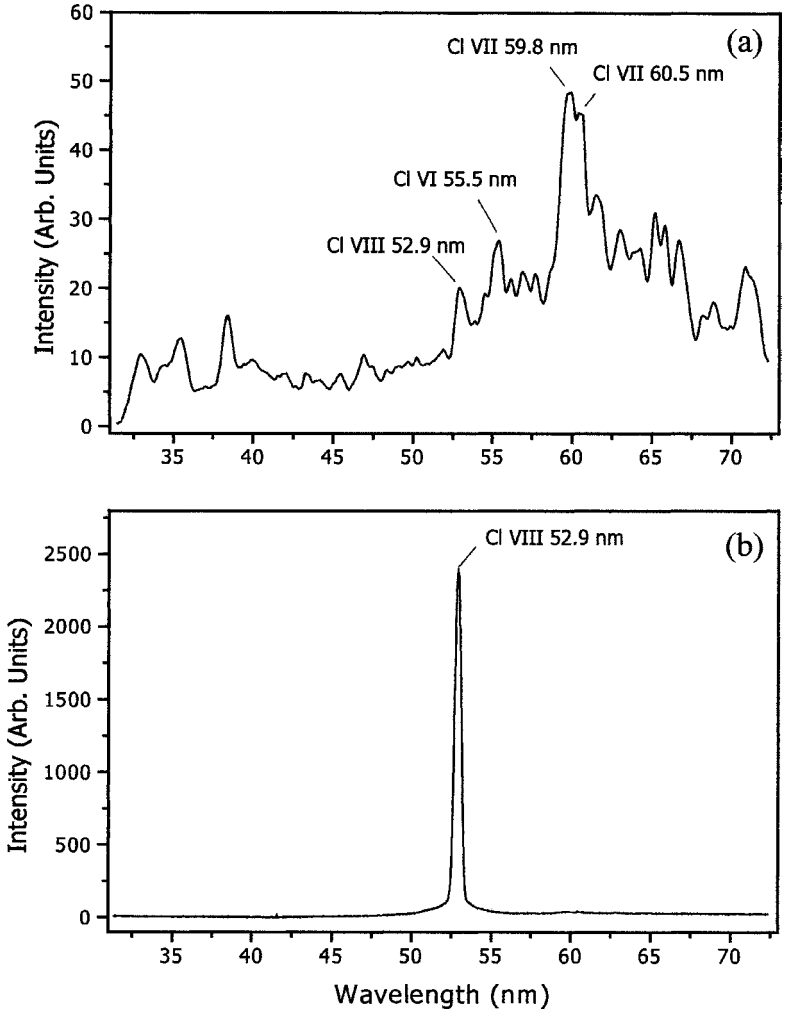

Figure 3. On-axis emission spectra of the Cl capillary discharge plasma in the region between 30 and 70 nm. (a) Spectrum corresponding to a 120 mTorr discharge. (b) Spectrum corresponding to a 224 mTorr discharge. In the latter, the dominance of the 59.2 nm Ne-like Cl transition is a clear indication of strong amplification.

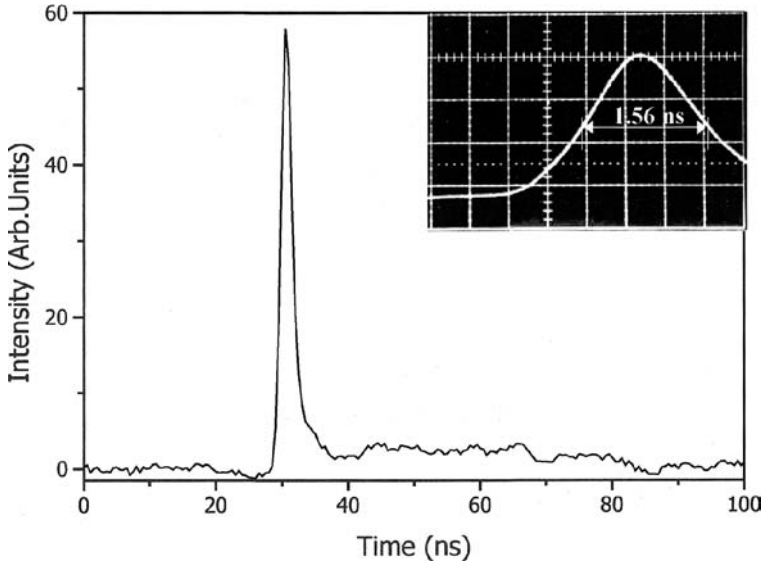

Figure 4. Temporal evolution of the 52.9 nm Ne-like Cl laser output pulse. The insert in the top right corner corresponds to the signal recorded with a fast vacuum photodiode and a 1-GHz bandwidth analog oscilloscope. The signal corrected for the limited bandwidth of the detection system yields a laser FWHM pulsewidth of 1.46 ns.

at this pressure, the intensity of this line is weak, smaller than that of several neighboring transitions of Cl VI and Cl VII, which cannot be inverted. A dramatic change in the spectrum is observed when the pressure is adjusted to 224 mTorr, the optimum pressure for lasing (*figure 3b*). At this pressure, the laser line is over two orders of magnitude more intense and completely dominates the entire 40 nm wide spectrum. This is clear evidence of large amplification in the 52.9 nm line.

The energy and temporal evolution of the laser output pulse were monitored with a vacuum photodiode. *Figure 4* shows a laser pulse with energy of 10 μJ measured operating the system at a repetition frequency of 0.5 Hz. The measurement of multiple shots yielded an averaged laser full width half maximum (FWHM) pulse of 1.46 ± 0.25 ns. The corresponding peak power is approximately 7 kW. However, the shot to shot variation in the laser pulse energy was significantly larger than those measured operating the laser at 46.9 nm using Ar [4,5]. The laser output pulse energy was also observed to deteriorate significantly at repetition rates greater than 1 Hz. This is probably due to insufficient gas renewal in the capillary channel, in which the reactive nature of excited Cl_2 gas leads to the buildup of contaminants. We also obtained a direct measurement of the beam divergence by recording the far-field pattern of the laser beam at 97 cm from the end of the capillary. The beam was observed to present maximum intensity on axis, and a FWHM divergence of approximately 4 mrad.

4. Applications

The recent demonstration of a compact saturated high repetition rate soft X-ray laser with pulse energy up to 1 mJ [4] opened the possibility of new applications for intense coherent short wavelength electromagnetic radiation in a table-top enviroment. Herein we discuss the results of soft X-ray interferometry of laser-created plasma using the combination of a novel amplitude division interferometer and a tabletop soft X-ray laser. We also summarize the first applications of a soft X-ray laser to materials diagnostics and laser ablation in a variety of metals.

4.1. Soft X-ray laser interferometry of dense plasmas

The development of gain-saturated soft X-ray lasers has opened the possibility to extend laser interferometry to large-scale plasmas of very high density that can not be probed with optical lasers [12]. The recent advent of gain-saturated tabletop soft X-ray lasers creates the opportunity of developing portable

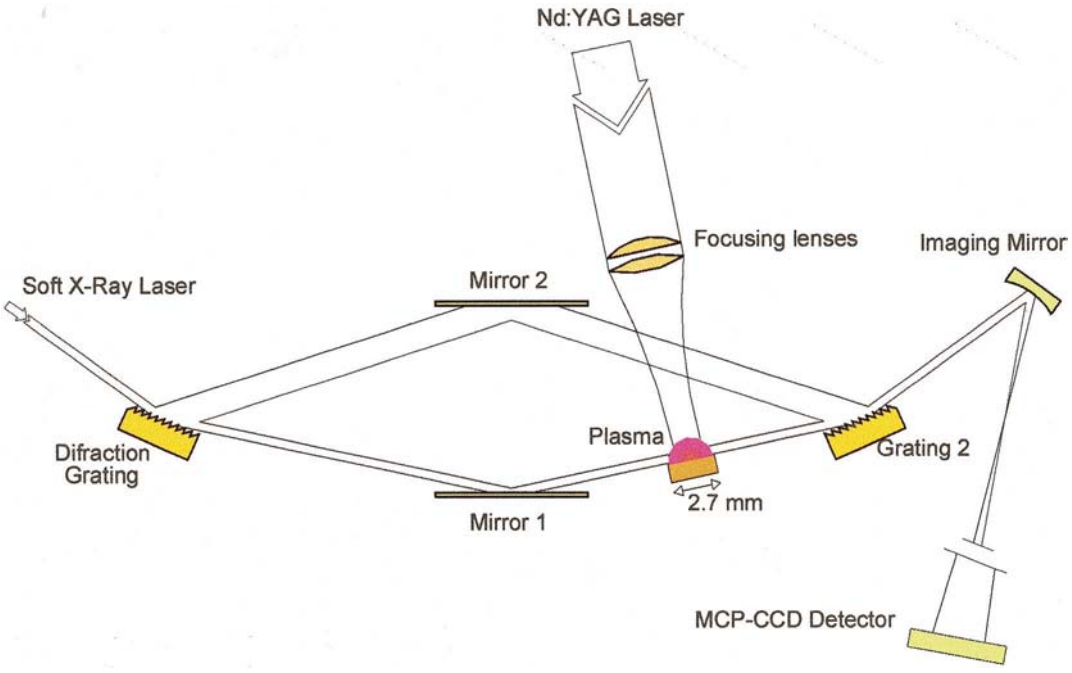

Figure 5. Schematic diagram of the soft X-ray grating interferometer and set-up for the diagnostic of a laser created plasma.

soft X-ray tools that will allow detailed maps of the electron density evolution in a great variety of very dense plasmas. Recently, our group has demonstrated plasma interferometry combining a 46.9 nm capillary discharge tabletop laser with a wavefront-division interferometer based on Lloyd's mirror [13,14]. The Lloyd's mirror has the advantage of constituting the simplest possible soft X-ray interferometer. However, it also presents some limitations: since this is a wavefront-division interferometer in which the fringe visibility relays on the spatial and temporal coherence of the laser, it is difficult to maintain good fringe visibility over a large area. To overcome this limitation we have developed a novel soft X-ray amplitude-division interferometer in which diffraction gratings are used as beam splitters in a Mach–Zehnder configuration. By properly tailoring the gratings this instrument can be made to operate at any selected soft X-ray wavelength.

The interferometer is schematically illustrated in *figure 5*. The soft X-ray laser beam is diffracted off the first grating into the two arms of the interferometer. The incidence angle and blaze of the grating are selected to allow for the laser radiation to be evenly split between the zero and first diffraction order. This is essential for obtaining a good fringe visibility. Two elongated grazing incidence mirrors are placed on the zero and first order arms of the interferometer to redirect the light towards the second grating, which recombines the beams to generate the interference pattern. The plasma to be studied is introduced in one of the arms of the interferometer. A Si/Sc multi-layer mirror [15] with 30 cm focal distance images the plasma into a MCP-CCD detector giving $25\times$ magnification [16]. A flat mirror (not shown in *figure 5*) was used to relay the image. The interferometer was pre-aligned using an IR-laser diode ($\lambda = 824$ nm) selected to have a temporal coherence length of ≈ 250 μm, similar to that of the soft X-ray laser. To allow the alignment of the interferometer with the semiconductor laser, the gratings were designed with two vertically separated rulings on the same substrate. Selecting the ratio of groove spacing equal to the ratio between the wavelengths of the semiconductor laser and soft X-ray lasers we obtained the same dispersion, and therefore the same optical path for both beams.

The interferometer was used in combination with the 46.9 nm capillary discharge tabletop laser to map the electron density evolution of a line-focused laser created plasma generated using a Cu slab target. The soft X-ray laser used in this experiment produces pulses with energies of about 0.13 mJ and 1.2 ns duration. The plasma under study was created focusing a Q-switch Nd : YAG laser operating at its fundamental wavelength of 1.06 μm into a ≈ 30 μm wide line focus ≈ 2.7 mm in length.

The results discussed below corresponds to the study of a plasma created with 0.36 J Nd : YAG laser pulses of ≈ 13 ns FWHM duration. *Figure 6a* shows a typical interferogram without the presence of the plasma, used as reference. Interferograms with very good fringe visibility (≈ 0.5) were obtained over the entire field of view. An interferogram with fringe shifts, produced by the presence of the plasma, is shown in *figure 6b*. This image was taken 12.5 ns after the start of the Nd : YAG laser pulse. The corresponding 2D electron density map is shown in *figure 6c*. By changing the delay between the Nd : YAG pulse and

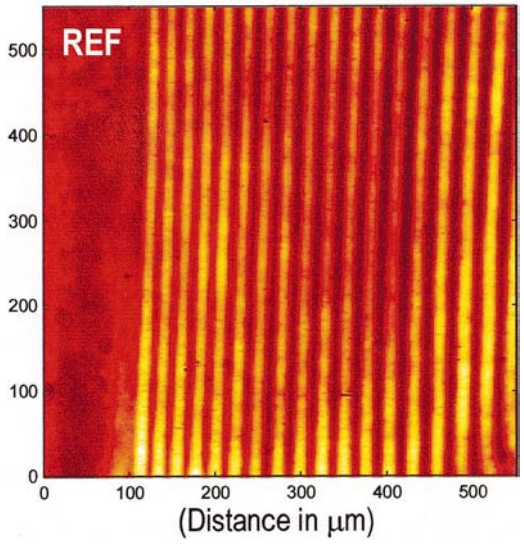

(a)

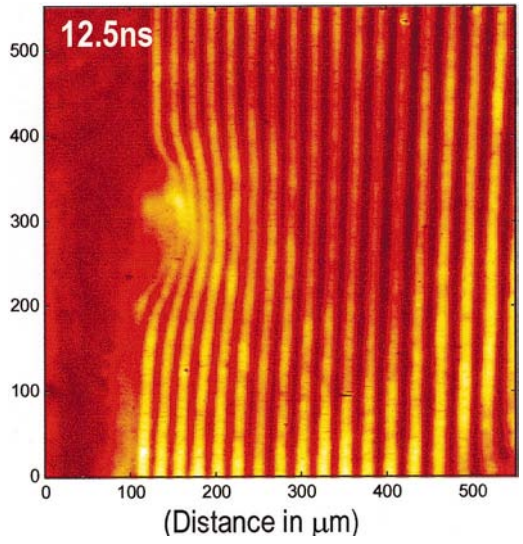

(b)

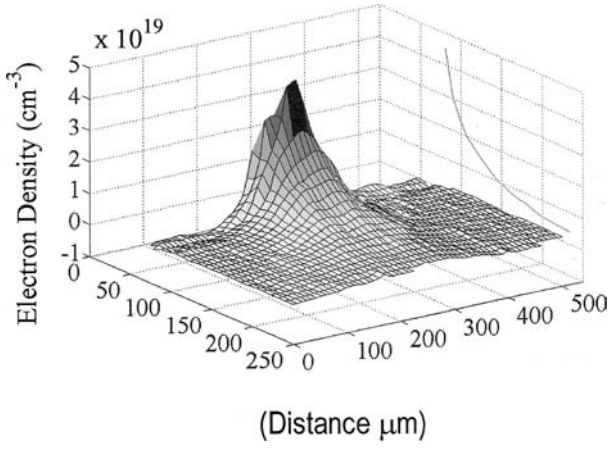

(c)

Figure 6. (a) Soft X-ray interferogram without the plasma present. (b) Interferogram of a 2.7 mm long line focus plasma generated by a Nd : YAG laser pulse ($\lambda = 1.06$ nm, 0.36 J, 13 ns FWHM) acquired 12.5 ns after the beginning of the Nd : YAG laser pulse. (c) Calculated density profile correspondig to the interferogram on (b).

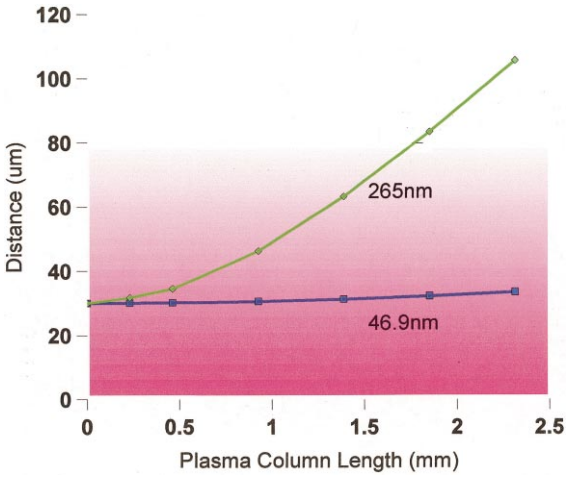

Figure 7. Computed trajectory of rays corresponding to a 46.9 nm (Ne-like Ar laser) and 265 nm (4th harmonic of Nd : YAG) traversing a plasma with electron density distribution corresponding to the 12.5 ns interferogram in *figure 6*.

soft X-ray laser pulse, we collected a sequence of interferograms that describe the entire evolution of the laser-created plasma [16].

We have been able to probe the plasma at locations as close as 25–30 μm from the target where the electron density is approximately $5 \cdot 10^{19}/\mathrm{cm}^3$, and the density gradient is steep. Another series of measurements for a 1.8 mm long line-focus plasma created by 0.6 J Nd : YAG laser pulses probed electron densities up to $1 \cdot 10^{20}/\mathrm{cm}^3$. Ray tracing computations show that these measurements would be difficult to realize with an UV laser probe due to strong refraction. The calculation, shown in *figure 7*, illustrates that while for the soft X-ray laser probe refraction at 30 μm of the target is small, the fourth harmonic of Nd : YAG is totally deflected out of the plasma.

4.2. X–UV reflectometry

The experimental setup used to perform reflectometry at 46.9 nm is shown in *figure 8*. The measurements were conducted in a vacuum chamber placed at about 1.5 m from the exit of the Ne-like Ar capillary discharge laser. The samples were mounted on the axis of a rotational stage driven by a stepper motor, which allowed for the selection of angles of incidence between 0 and 90 degrees. The intensity of the reflected beam was recorded with a vacuum photodiode (labeled A in *figure 8*), that was mounted on a lever arm that followed the angular motion of the reflected beam. A 1 mm diameter pinhole was placed at the entrance of the chamber to reduce the spot size of the laser beam incident on the sample, which allowed for measurements at grazing angles approaching zero degrees. To overcome scattering of the data due to shot to shot intensity variation of the laser, the intensity of the reflected beam was normalized by the intensity of the incident beam for each laser pulse. For this purpose a reference beam was generated by placing a 50% transmissive gold-plated grid in the path of the incident beam. The intensity of the reference beam reflected by the grid was measured by a second fixed vacuum photodiode (labeled B in *figure 8*). The angular dependence of the reflectivity was measured by scanning the angle of incidence while repetitively firing the laser at a repetition frequency of 1 Hz.

Figure 9 is an example of the reflectance data obtained. It shows the reflectivity as a function of incident angle for a bulk crystalline sample of InP with a 100 orientation. This data depicts a typical measurement run that consisted of 300 contiguous laser pulses for a 90 degree rotation of the sample. At small angles of incidence, photodiode A blocks the beam from impinging on the sample limiting the minimum angle at which data could be obtained to 1.6 degrees. This angle, which corresponds to the first valid data point near normal incidence, was determined from the geometric dimensions of the system and was used to relate each data point to its corresponding angle. At the other extreme, as the incident angle approaches 90 degrees,

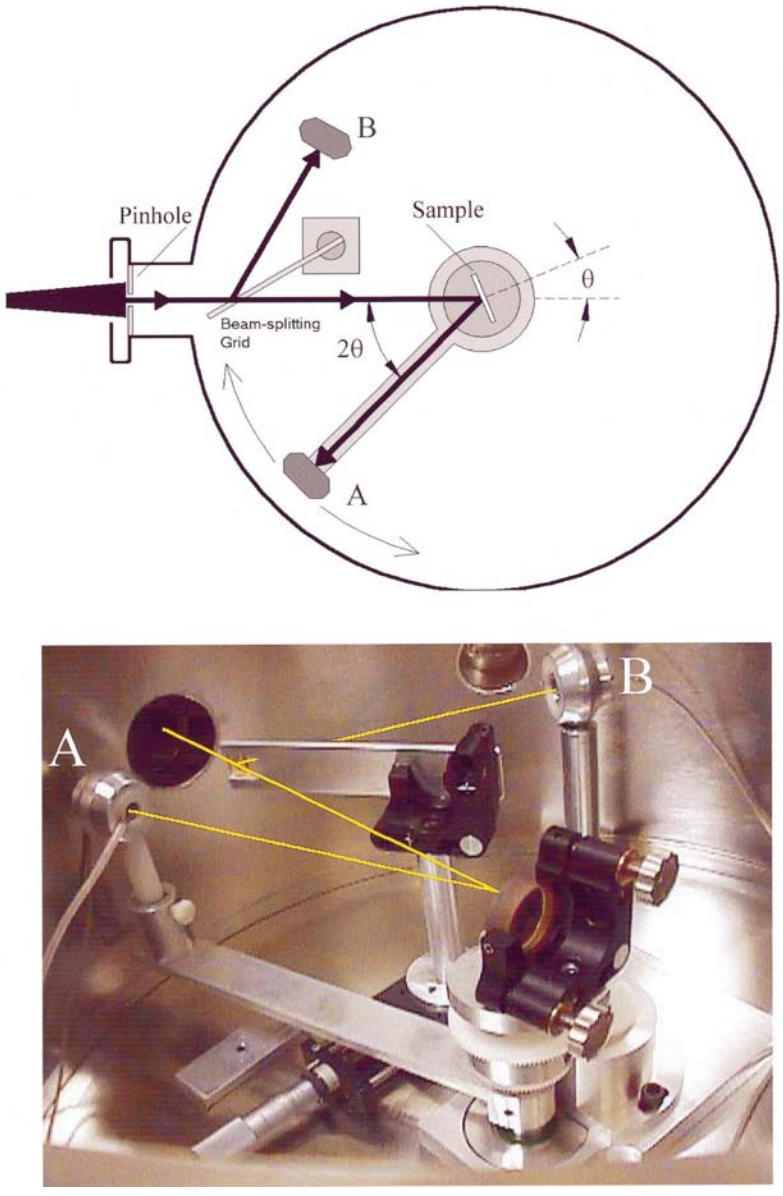

Figure 8. Schematic diagram of the laser reflectometer used in the measurement of X–UV optical constants of materials.

the projection of the incident beam on the sample becomes larger than the sample and therefore limited the maximum angle at which valid data could be obtained.

4.2.1. *Determination of optical constants of materials*

The optical constants for Si, GaP, InP, GaAs, GaAsP and Ir at a wavelength of 46.9 nm (26.5 eV) were obtained by fitting the measured angular dependence of the reflectivity with the Fresnel formula. The results are sumarized in *table 2*. The high intensity of the laser source is an advantage for the accurate measurement of the reflectivity at near normal incidence where the reflectivity of most materials is low. Our analysis of

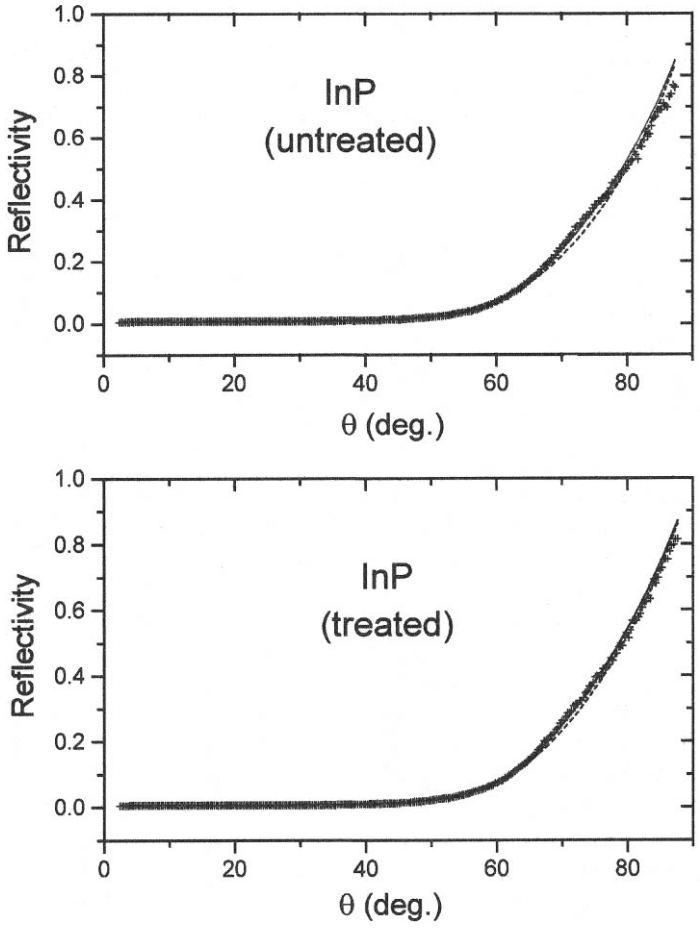

Figure 9. Measured and calculated reflectivity for 100 crystalline InP as a function of incident angle θ. (a) Before chemical treatment. The dotted curve corresponds to: $\tilde{n}_{\mathrm{b}} = 0.92 + i \cdot 0.14$ without the surface layer, the solid curve considering a surface layer: $\tilde{n}_{\mathrm{b}} = 0.88 + i \cdot 0.087$ (layer: $\tilde{n}_{\mathrm{l}} = 0.82 + i \cdot 0.39$, thickness $d_{\mathrm{l}} = 1.8$ nm). (b) After chemical treatment. The dotted curve corresponds to: $\tilde{n}_{\mathrm{b}} = 0.91 + i \cdot 0.13$ without the surface layer, the solid curve considering a surface layer: $\tilde{n}_{\mathrm{b}} = 0.88 + i \cdot 0.09$ (layer: $\tilde{n}_{\mathrm{l}} = 0.84 + i \cdot 0.26$, thickness $d_{\mathrm{l}} = 2.5$ nm).

Table 2. Summary of optical constants at 26.5 eV measured using X–UV reflectometry. Previously measured values from [23] are also listed

No	Sample	Treated	This work		Ref. [10]	
			n	k	n	k
1	Si	No	0.82	0.015	0.803	0.0178
2		Yes	0.80	0.021		
3	GaP	No	0.82	0.052	N/A	0.100
4		Yes	0.82	0.055		
5	InP	No	0.88	0.087	N/A	N/A
6		Yes	0.89	0.090		
7	GaAs	No	0.84	0.060	N/A	0.083
8	GaAsP	No	0.83	0.059		
9	Ir	No	0.81	0.53	0.67	0.69

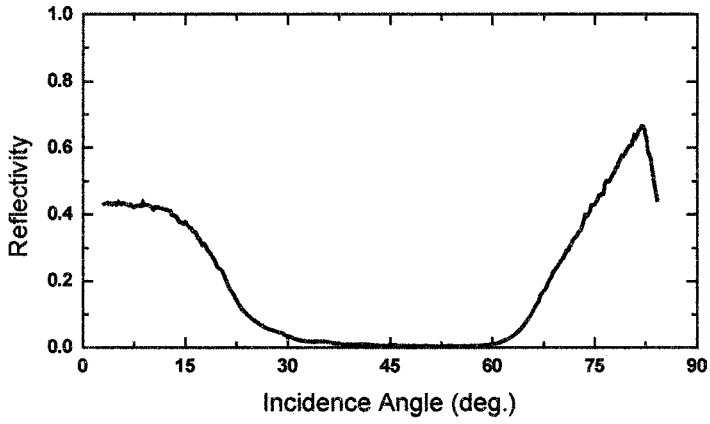

Figure 10. Measured reflectivity of a Si/Sc multilayer mirror at 46.9 nm as a function of incidence angle.

the data made use of models that take into account the presence of a surface layer of contamination, which develops on most materials in a natural atmospheric environment. In order to fully characterize the influence of the surface layer on the measurement, the samples were chemically treated in the following manner to alter the characteristics of the surface layer. The samples were dipped in a 5% solution of HF in distilled water for approximately 5 min and were then rinsed with acetone and methanol. The samples were exposed to ambient atmospheric conditions for less than 5 minutes before being positioned in the system under a vacuum of about $1 \cdot 10^{-5}$ Torr. Measurement of the treated and untreated samples that had different surface layer characteristics gave similar optical constants for the bulk material. This suggests that the approach used in this work is capable of yielding reliable values of the optical constants for the bulk material in the presence of surface layer contaminants. The measurements of the optical constants of InP and GaAsP constitute, to the best of our knowledge, the first experimental values at this wavelength, while for the rest of the materials, the values obtained are in most cases in good agreement with tabulated values. These measurements and the analysis of the data are discussed in more detail in a recent paper [17].

4.2.2. *Angular dependent reflectivity of Si/Sc multilayer mirror*

Utilizing the experimental setup described above, measurements were made to determine the angular dependent reflectivity of Si/Sc multi-layer mirrors designed for use at a wavelength of 46.9 nm. The multilayer coatings were deposited on super-polished borosilicate substrates by dc magnetron sputtering with a period of 18–27 nm and a ratio of layer thickness $H(\mathrm{Sc})/H(\mathrm{Si}) = 0.786$. The mirror parameters have been discussed in detail previously [15]. As an example, *figure 10* shows the measured reflectivity as a function of incidence angle for a mirror designed to operate at normal incidence. The graph corresponds to the average of four runs. The runs varied in the number of data points collected from 200 to 400 for a scan angle of 90 degrees. Each individual run yielded very similar data and the averaging was used only to reduce the random noise in the measurement. A near normal incidence reflectivity of 43% was measured at 1.6 degrees.

4.3. Soft X-ray laser ablation

Focused soft X-ray laser beams have the potential to reach very high intensities and energy densities, opening new applications for short wavelength coherent electromagnetic radiation. Preliminary results of an attempt to focus laser pulses from a collisional soft X-ray laser pumped by a large optical laser have been reported [18]. In this section we summarize the characterization of a focused 46.9 nm laser beam generated by a Ne-like Ar capillary discharge soft X-ray laser, and the results of the first laser ablation experiment with a soft X-ray laser.

The experimental setup used to focus the laser beam and characterize its intensity distribution in the focal region is shown in *figure 11*. The soft X-ray laser pulses had an energy of about 0.13 mJ and 1.2 ns

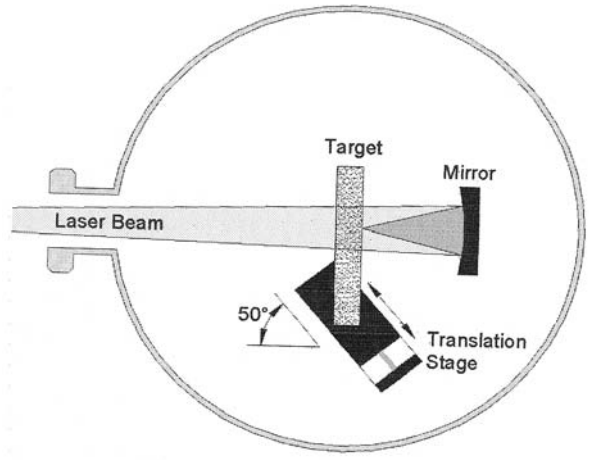

Figure 11. Experimental setup used to focus the soft X-ray laser beam.

FWHM duration and were generated at a repetition rate of 1 Hz by amplification in a 18.2 cm long Ar capillary plasma. The far field beam profile has been measured to have an annular shape with a peak to peak divergence of about 4.6 mrad [5]. This annular intensity distribution is caused by refraction of the rays in the amplifier due to radial density gradients [19,20]. The laser beam was focused by a spherical ($R = 10$ cm) Si/Sc multilayer-coated mirror located in a vacuum chamber at 256.5 cm from the exit of the capillary discharge amplifier. The mirror used in this experiment has a normal incidence reflectivity of $\approx 40\%$ at 46.9 nm. The mirror was positioned at normal incidence with the purpose of minimizing aberrations. Therefore, the reflected beam was focused on axis, where it impinged on the flat face of a target consisting of a thin (2 mm thick) metal strip.

The focused laser beam was observed to have sufficient intensity to ablate aluminum, stainless steel and brass when the samples are positioned within several hundred μm from the focus. The characteristics of the imprints on the metal surface depend not only on the intensity distribution, but also on the melting point and heat conductivity of the sample, and on the duration of the laser pulse [21]. Nevertheless, they can give useful two-dimensional information of the focused laser beam intensity distribution. To map the evolution of the laser intensity distribution along the propagation axis we mounted the target on a translation stage driven by a computer controlled stepper motor. The axis of motion of the translation stage was positioned at an angle with respect to the optical axis. Series of imprints of the beam for positions along the optical axis were obtained by continuously moving the translation stage while repetitively firing the laser at a repetition rate of 1 Hz.

Figure 12 is a scanning electron microscope (SEM) photograph of the surface of a brass target showing the progression of ablation patterns obtained as the target was moved away from the mirror towards the focus. Each ablation pattern is the result of a single laser shot. At an axial distance of a few hundred μm from the focal region the ablation patterns have the shape of thin annular disks. These rings show good azimuthal symmetry, except for a small discontinuity where the incoming beam was blocked by the target. As the focal region is approached the thickness of the ablated rings increases, and a central spot develops. The depth of the rings was measured to be ≈ 2 μm using a Zygo interferometer. Finally, very near the focus the patterns evolve into a single spot with a deep hole on axis. The smallest spot has an outer diameter of about 17 μm and contains a deep central hole of about 2–3 μm diameter.

To increase the understanding of the characteristics of the laser beam in the focal region and to obtain an estimate of the power density deposited we analyzed these results with ray-tracing computations. *Figure 13* shows the computed radial cross section of the beam intensity distributions in the focal region. For comparison with the experiment the measured boundaries of the ablated regions are represented as

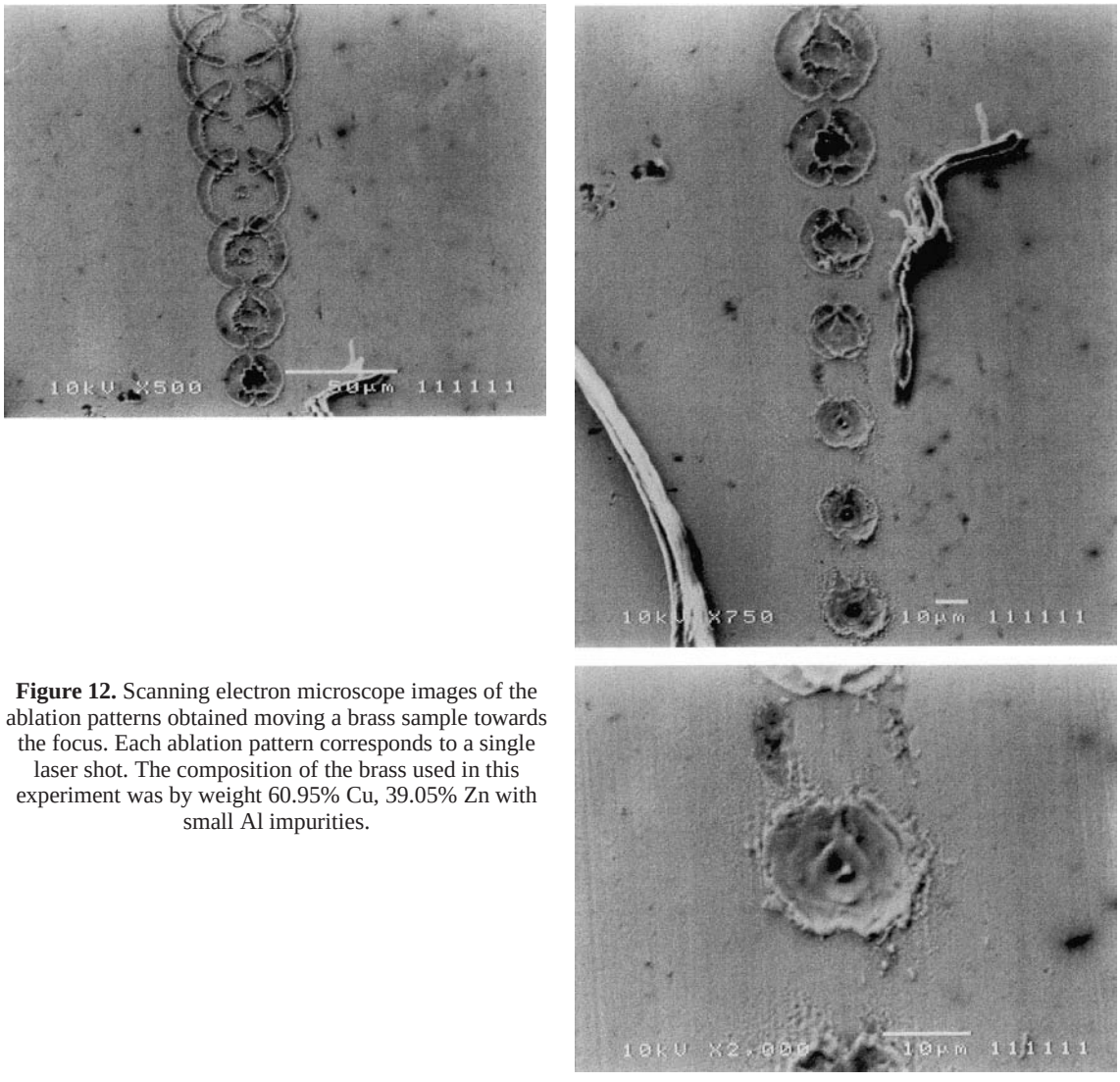

Figure 12. Scanning electron microscope images of the ablation patterns obtained moving a brass sample towards the focus. Each ablation pattern corresponds to a single laser shot. The composition of the brass used in this experiment was by weight 60.95% Cu, 39.05% Zn with small Al impurities.

black dots in the same figure. All the major features of the observed ablation profiles of *figure 12* are well described by the ray tracing computations. The computations show that at a few hundred µm from the focal region the highest concentration of rays defines a thin ring. Also in accordance with the experiment a central peak is observed to develop as the focal region is approached. Both features are the result of the spherical aberration that causes the rays to converge and cross at those locations. Similarly, the spherical aberration causes the central peak, which begins to develop when the outermost rays converge on the axis. Near the so-called 'plane of minimum confusion' the intensity distribution is computed to be dominated by the sharp central peak, which is responsible for the deep central hole observed in the SEM. The average intensity within a 2 µm diameter region is estimated to be greater than $1 \cdot 10^{11}$ W/cm^2 from the computed fraction of rays that intersect this region. The analysis also confirms that the minimum spot size obtained in this experiment is dominantly limited by the spherical aberration. Exposure of the targets to multiple laser shots in each position is observed to result in the ablation of deep holes. As an example, *figure 14* (left) shows a sequence of ablation patterns obtained in aluminum using 40 laser shots for each target position.

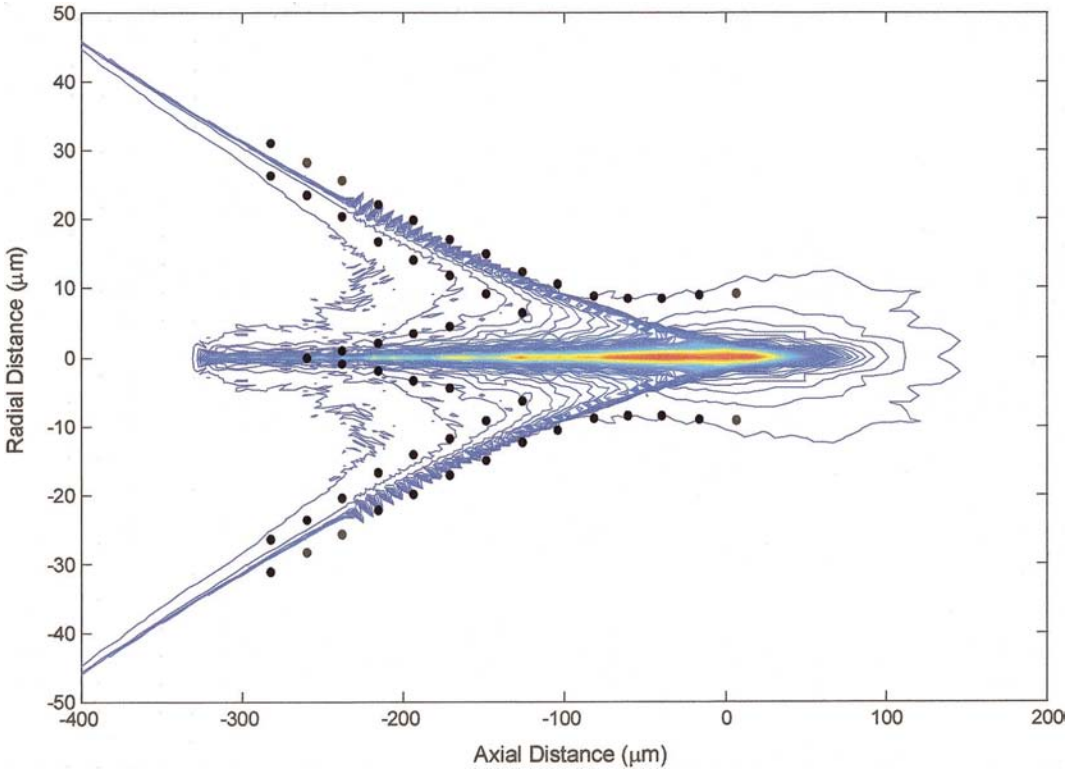

Figure 13. Computed radial cross section of the beam in the focal region. The dots correspond to the measured boundaries of the ablated patterns.

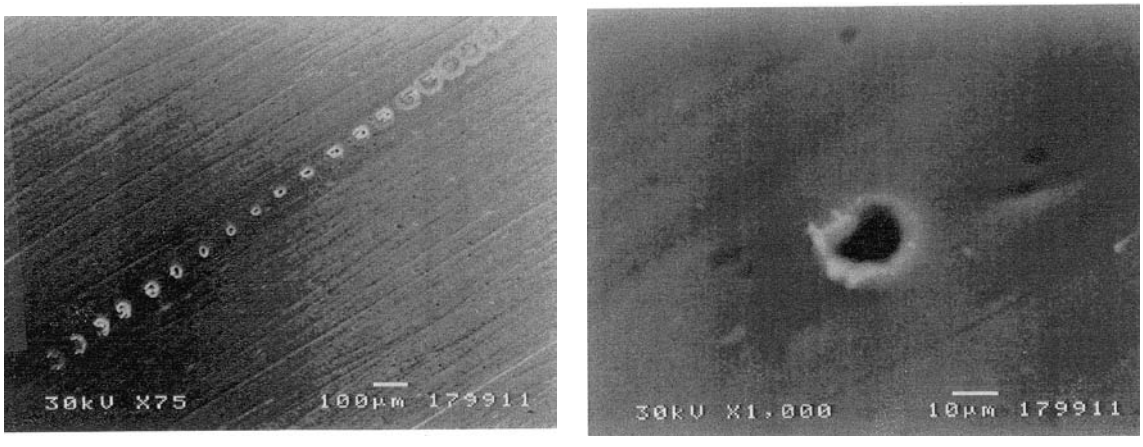

Figure 14. Scanning electron microscope images of ablation patterns on aluminum obtained by moving the sample near the location of the focus (left). Ablation hole resulting from 40 shots near the focus (right).

Figure 14 (right) is a SEM image of an ablation hole near the focus, which is seen to have a diameter on the order of 10 μm. The focusing setup used in this experiment was different from that shown in *figure 14*. The beam was first reflected using a Si/Sc multilayer mirror that has a 3 mm diameter hole at its center

and was then focused back through the hole onto the target using a spherical Si/Sc multilayer mirror with radius of curvature $R = 20$ cm [22]. While the flat mirror introduces an additional loss due to the $\approx 40\%$ reflectivity, the intensity is still well above the threshold for ablation of metals when the sample is located within several hundred μm from the focal position.

5. Conclusions

Capillary discharge-pumped lasers are the first tabletop soft X-ray lasers to reach a level of development that allows their routine use in numerous applications. The average coherent power per unit of spectral bandwidth of the Ne-like Ar laser is similar to that of a third generation synchrotron beam line, and its high peak spectral brightness makes it one of the brightest sources of soft X-ray radiation. We have used this very compact discharge pumped 46.9 nm laser in combination with an amplitude division interferometer to probe a large-scale laser created plasma. This result may lead to the use of table-top soft X-ray lasers in probing a great variety of dense plasmas. In a separate experiment we took advantage of the high repetition rate of the capillary discharge laser to conduct reflectivity measurements as a function of angle. These measurements resulted in the determination of optical constants at $\lambda = 46.9$ nm for several materials, and in the characterization of XUV multilayer mirrors. One of these mirrors was subsequently used to focus the beam of a table-top Ne-like Ar soft X-ray laser, realizing the first demonstration of material ablation with a coherent soft X-ray beam. These proof of principle experiments in materials science and plasma diagnostics show that tabletop capillary discharge lasers are a powerful sources of coherent short-wavelength radiation that can impact numerous fields.

Acknowledgements. The development of the soft X-ray laser was supported by the National Science Foundation. The plasma interferometry work was supported by the US Department of Energy grant DE-FG03–98DP00208. We also acknowledge the support of the Colorado CPOP program, and the US Civilian Research and Development Foundation (CRDF) for the collaboration that resulted in the development of the multi-layer mirrors. M. Marconi acknowledges the support of CONICET. We are thankful M. Forsythe, J.L.A. Chilla and Yu.A. Unspenskii for their important contributions, and to O.E. Martinez for helpful discussions.

[1] Permanent address: FCEyN, UBA, Argentina.

References

[1] Rundquist A., Durfee III C.G., Chang Z., Herne C., Backus S., Murnane M.M., Kapteyn H.C., Phase-matched generation of coherent soft X-rays, Science 280 (1998) 1412.
[2] Spielmann Ch., Burnett N.H., Sartania S., Koppitsch R., Schnürer M., Kan C., Lenzer M., Wobrauschek P., Krausz F., Generation of coherent X-rays in the water window using 5-femtosecond laser pulses, Science 278 (1997) 661.
[3] Rocca J.J., Tabletop soft X-ray lasers, Rev. Sci. Instrum. 70 (1999) 3799.
[4] Macchietto C.D., Benware B.R., Rocca J.J., Generation of millijoule-level soft X-ray laser pulses at 4-Hz repetition rate in highly saturated tabletop capillary discharge amplifier, Opt. Lett. 24 (1999) 1115.
[5] Benware B.R., Macchietto C.D., Moreno C.H., Rocca J.J., Demonstration of a high average power table-top soft X-ray laser, Phys. Rev. Lett. 81 (1998) 5804.
[6] Liu Y., Seminario M., Tomasel F.G., Chang C., Rocca J.J., Attwood D.T., High Average power soft X-ray laser beams approaching full spatial coherence, Science (2000), submitted.
[7] Foltin M., Stueber G.J., Bernstein E.R., On the growth dynamics of neutral vanadium oxide and titanium oxide clusters, J. Chem. Phys. 111 (21) (1999) 9577.
[8] Frati M., Seminario M., Rocca J.J., Demonstration of a 10 micro-joule tabletop laser at 52.9 n in neon-like chlorine, Opt. Lett., in press.
[9] Li Y., Pretzler G., Fill E.E., Ne-like ion lasers in the extreme ultraviolet region, Phys. Rev. A 52 (1995) R3433.
[10] Rocca J.J., Shlyaptsev V.N., Tomasel F.G., Cortazar O.D., Hartshorn D., Chilla J.L.A., Demonstration of a discharge pumped tabletop soft X-ray laser, Phys. Rev. Lett. 73 (1994) 2192.

[11] Rocca J.J., Clark D.P., Chilla J.L.A., Shlyaptsev V.N., Energy extraction and achievement of the saturation limit in a discharge pumped table-top soft X-ray laser, Phys. Rev. Lett. 77 (1996) 1476.
[12] Da Silva L.B., Barbee Jr. T.W., Cauble R., Celliers P., Ciarlo D., Libby S., London R.A., Matthews D., Mrowka S., Moreno J.C., Ress D., Trebes J.E., Wan A.S., Weber F., Electron density measurements of high density plasmas using soft X-ray laser interferometry, Phys. Rev. Lett. 74 (1995) 3991.
[13] Rocca J.J., Moreno C.H., Marconi M.C., Kanizay K., Soft X-ray laser interferometry of a plasma with a table-top laser and Lloyd's mirror, Opt. Lett. 24 (1999) 420.
[14] Moreno C.H., Marconi M.C., Kanizay K., Rocca J.J., Unspenskii Yu.A., Vinogradov A.V., Pershin Yu.A., Soft X-ray interferometry of a pinch discharge using a tabletop laser, Phys. Rev. E 60 (1999) 911.
[15] Uspenskii Yu.A., Levashov V.E., Vinogradov A.V., Fedorenko A.I., Kondratenko V.V., Pershin Yu.P., Zubarev E.N., Fedotov V.Yu., High reflectivity multilayer mirrors for a vacuum-ultraviolet interval of 35–50 nm, Opt. Lett. 23 (1998) 771.
[16] Filevich J., Kanizay K., Marconi M.C., Chilla J.L.A., Rocca J.J., Dense plasma diagnostics with an amplitude-division soft-X-ray laser interferometer based on diffraction gratings, Opt. Lett. 25 (5) (2000) 356.
[17] Artioukov I.A., Benware B.R., Rocca J.J., Forsythe M., Uspenskiia Yu.A., Vinogradov A.V., Determination of XUV optical constants by reflectometry using a high repetition rate 46.9 nm laser, IEEE J. Sel. Topics Quantum Electron. 5 (1999) 1495.
[18] Zeitoun Ph., Sebban S., Murai K., Tang H. et al., Experimental investigation of X-ray laser focusability using bragg-fresnel reflective lens, in: Y. Kato, H. Takuma, H. Daido (Eds.), X-ray Lasers 1998, IOP Conf. Proc., Vol. 159, Institute of Physics, Bristol and Philidelphia, 1998, pp. 6770.
[19] Moreno C.H., Marconi M.C., Shlyaptsev V.N., Benware B.R., Macchietto C.D., Chilla J.L.A., Rocca J.J., Osterheld A.L., Two-dimensional near-field and far-field imaging of a Ne-like Ar capillary discharge table-top soft X-ray laser, Phys. Rev. A 58 (1998) 1509–1514.
[20] Chilla J.L.A., Rocca J., Beam optics of gain-guided soft-X-ray lasers in cylidrical plasmas, J. Opt. Soc. Am. B 13 (1996) 12.
[21] Miller J.C., Haglund R.F., Laser Ablation and Desorption, Academic, San Diego, CA, 1998.
[22] Benware B.R., Rocca J.J., Ozols A., Machietto C.D., Chilla J.L.A., Artioukov I.A., Kasjanov Yu.S., Kodratenko V.V., Vinogradov A.V., Applications of a high repetition rate table top soft X-ray laser: laser ablation with a focused beam and reflectometry of materials, in: J.J. Rocca, L.B. Da Silva (Eds.), Proceedings of SPIE, Vol. 3776.
[23] Palik E.D., Handbook of Optical Constants of Solids, Academic Press, San Diego, CA, 1998.